A NUMERICAL SIMULATION OF DIURNAL VARIATIONS OF METEOROLOGICAL FIELDS IN SUMMER

Qian Yongfu (钱永甫) and *Wang Qianqian* (王谦谦)
Lanzhou Institute of Plateau Atmospheric Physics, Academia Sinica, Lanzhou

Received July 21, 1983

ABSTRACT

The influences of the Tibetan Plateau and the Rocky Mountains on diurnal variations of the meteorological fields in July are investigated by use of a five-layer global atmospheric general circulation model which includes various physical processes, including diurnal variation of solar radiation and real topography. In this paper, a brief description of the model is given first and then we emphatically discuss the results by comparatively analysing the influences of the Tibetan Plateau and the Rocky Mountains on diurnal changes of temperature, the geopotential height, the horizontal and the vertical flows, as well as the vertical circulations in summer. The comparative analyses show that there are very prominent diurnal variations of temperature, geopotential height, wind fields and vertical circulations in the mountainous regions, the amplitudes of their variations are proportional to the scales of topography.

I. INTRODUCTION

Ye and Gao have pointed out in their book [1] that there are very prominent phenomena of diurnal variations of meteorological fields in mountainous areas both in summer and in winter. As has been demonstrated by Kuo and Qian [2], those diurnal variations are undoubtedly caused by the great differences of the thermal effects of elevated Plateau surfaces during daytime and nighttime. In order to depict the diurnal process Kuo and Qian have used a limited area primitive equation model to study the influences of the Tibetan Plateau on diurnal variations of meteorological fields in that very area and its vicinities [2]. Their simulation area includes Euroasia, most areas of Africa and some parts of Australia in 0°—180° E and 25°S—55°N. Because of the boundary effect in their model, some results near the boundaries are not very reasonable when the integration time increases. In order to overcome the disadvantage of their model, we extend the model to cover the whole globe. Therefore, the Tibetan Plateau and the Rocky Mountains are naturally included in the experimental region, we can compare their effects on diurnal changes of meteorological fields.

In this paper, we shall briefly introduce the global model, and then focus our attention on the discussions of the influences of the Tibetan Plateau and the Rocky Mountains on diurnal variations of temperature, horizontal and vertical flow fields.

II. A BRIEF INTRODUCTION OF THE GLOBAL MODEL

1. *Governing Equations*

The model we used in this work is nearly the same as the one Kuo and Qian used before[2,3] which is developed from the model of Qian et al.[4] and treats the top layer of the atmosphere from $p=0$ to $p=p_c$ in ordinary p-coordinate, the layer from p_c to $p_s-\Delta p_b$ in σ-coordinate and the bottom layer of constant pressure thickness Δp_b in dimensionless pressure σ_b-coordinate, where p_s is the surface

pressure and σ, σ_b are defined by

$$\sigma=\frac{p-p_c}{p_s^*}, \qquad \sigma_b=\frac{(p+\Delta p_b-p_s)}{\Delta p_b}. \qquad (p_s^*=p_s-p_c-\Delta p_b) \tag{1a,b}$$

Specifically, we use $p_c=400$ mb and $\Delta p_b=50$ mb and divide the top layer into two layers of equal pressure thickness $\Delta p=p_c/2$, the p_c to $p_s-\Delta p_b$ layer into two layers of equal σ-thickness $\Delta\sigma=1/2$ and treat the lowest layer of 50 mb thickness as a single surface boundary layer which interacts directly with the top layer of the ground or ocean which is treated as the sixth layer of the model.

For simplicity, we write the prognostic equations for the horizontal velocity vector $\boldsymbol{V}$, temperature T and water vapor mixing ratio q, the continuity and the hydrostatic equation for the atmosphere in σ-coordinate in the following forms

$$\frac{d\boldsymbol{V}}{dt}=-PG-f\,K\times\boldsymbol{V}+D_v, \tag{2}$$

$$\frac{dT}{dt}=\frac{RT}{p_{c_p}}[\omega+\varepsilon_s+\varepsilon_{IR}+L(C_l+C_c)]+D_T, \tag{3}$$

$$\frac{dq}{dt}=-C_l-C_c+D_q, \tag{4}$$

$$\frac{\partial p_s^*}{\partial t}=-\nabla\cdot p_s^*\,\boldsymbol{V}-\frac{\partial p_s^*\,\dot\sigma}{\partial\sigma}, \tag{5}$$

$$\frac{\partial\varphi}{\partial\sigma}=-\frac{RT}{\sigma+\dfrac{p_c}{p_s^*}}, \tag{6}$$

where PG is the horizontal pressure gradient force, D_v, D_T and D_q are the net eddy transports of velocity, temperature and mixing ratio, ε_{IR} and ε_s are the diabatic heating rates from infrared and solar radiations, C_l and C_c are the large scale and cumulus condensation rates, L is the latent heat of condensation, $\omega=dp/dt=p_s^*\,\dot\sigma+\sigma\dot p_s^*$, and ϕ is the geopotential height. For convenience, we combine (2), (3) and (4) with (5) to reduce the individual changes into local changes and net fluxes, viz.,

$$\frac{dX}{dt}=\frac{\partial X}{\partial t}+\frac{1}{p_s^*}\left[\nabla\cdot p_s^*\,X\,\boldsymbol{V}+\frac{\partial p_s^*\,X\dot\sigma}{\partial\sigma}+X\frac{\partial p_s^*}{\partial t}\right], \tag{7}$$

where X represents either $\boldsymbol{V}$, T or q. The equations for the top layers in p-coordinate and those for the surface layer can also be represented by these equations by setting $p_c=0$, $p_s^*=1$ and $\sigma=\sigma_b$, $p_c=p_s-\Delta p_b$, respectively.

From the definitions of σ and σ_b and the continuity equation, we find

$$\dot\sigma_0=\frac{\omega(p_c)}{p_s^*}=-\frac{p_c}{2p_s^*}\nabla\cdot(V_1+V_2), \tag{8a}$$

$$\dot\sigma_{bo}=\nabla\cdot V_5, \qquad \dot\sigma_{b1}=0, \tag{8b,c}$$

$$\dot\sigma_1=\frac{\Delta p_b}{p_s^*}\dot\sigma_{b0}=\frac{\Delta p_b}{p_s^*}\nabla\cdot V_5, \tag{8d}$$

where the subscripts 0 and 1 of $\dot\sigma$ and $\dot\sigma_b$ refer to the values of σ and σ_b, respectively. A $\bar X$ and $\bar X^2$

conserving difference scheme will be used in calculating the fluxes in (7).

To find $\dot{\sigma}_{\frac{1}{2}}$, we apply $\partial/\partial\sigma$ to (5) and make use of the fact that p_s^* is independent of σ to arrive at the following equation

$$\frac{1}{p_s^*}\nabla\cdot(p_s^*\frac{\partial V}{\partial\sigma})+\frac{\partial^2\dot{\sigma}}{\partial\sigma^2}=0. \tag{9}$$

Replacing the differentials by centered differences at $\sigma=1/2$, we then obtain

$$\begin{aligned}\dot{\sigma}_{\frac{1}{2}}&=0.5\,[\dot{\sigma}_0+\dot{\sigma}_1+\frac{1}{2p_s^*}\nabla\cdot(V_4-V_3)\,p_s^*\,]\\&=\frac{1}{4p_s^*}\,[2\Delta p_b\,\nabla\cdot V_5+\nabla\cdot p_s^*(V_4-V_3)-p_c\nabla\cdot(V_1+V_2)]\,.\end{aligned} \tag{9a}$$

We eliminate $\dot{\sigma}$ from (5) by applying it to $\sigma=0.75$ and substituting $\dot{\sigma}_1$ and $\dot{\sigma}_{\frac{1}{2}}$ from (8d) and (9a) into it. The result is

$$\frac{\partial p_s}{\partial t}=-\frac{1}{2}[p_c\nabla\cdot(V_1+V_2)+\nabla\cdot p_s^*(V_3+V_4)+2\Delta p_b\nabla\cdot V_5]\,. \tag{10}$$

As has been mentioned before, we also include the top layer of the land and ocean in our model as the sixth layer under the assumption that it is at rest.We choose the depth z^* of this underlying layer just large enough to have the heat flux h_{z^*} at this level nearly equal to zero. Then the change of the mean temperature T_G of this layer is given by

$$\frac{\partial T_G}{\partial t}=\frac{1}{\rho_e C_e z^*}\,h_s\,, \tag{11}$$

where ρ_e and C_e are the density and heat capacity of this layer and h_s is the downward heat flux at the surface. We approximate T_G by the temperature of the underlying medium at the mid-level $z_e=z^*/2$ and calculate h_s by the following equation

$$h_s=2\rho_e C_e K_e(T_s-T_G)/z^*\,, \tag{12}$$

where K_e is the conduction coefficient of the medium and T_s is the surface temperature. Eq. (11) then becomes

$$\frac{\partial T_G}{\partial t}=\lambda_e(T_s-T_G)\,, \tag{13}$$

where $\lambda_e=2K_e/z^{*2}$. We take $K_e=2.8\times10^{-3}\,\mathrm{cm^2\,s^{-1}}$, $z^*=40$ cm for land and take $z^*=100$ cm and $R_e=2.0\ \mathrm{cm^2 s^{-1}}$ for the oceans, so that we have

$$\lambda_e=3.5\times10^{-6}\mathrm{s^{-1}},\quad \text{for land;}\qquad \lambda_e=4.0\times10^{-4}\mathrm{s^{-1}},\quad \text{for ocean.} \tag{13a,b}$$

2. *Diffusion and Flux Calculations*

The net eddy transport term D_x of the quantity X in equations (2)–(4) is given by the Fickian diffusion formula, i.e.

$$D_X = K_h \nabla_h^2 X - g \frac{\partial \tau_X}{\partial p}, \tag{14}$$

where X stands for either V, T or q, K_h is the effective horizontal diffusion coefficient which is taken to be nearly equal to 10^6 m^{2}s^{-1} for the $\Delta\lambda = \Delta\varphi = 5°$ grid size chosen, and τ_X is the downward flux of X and is expressed as

$$\tau_X = -g\rho^2 K_z \frac{\partial X}{\partial p}, \qquad \text{in the atmosphere,} \tag{14a}$$

and

$$\tau_X = \rho_s C_D |V_s| (X_b - X_s), \qquad \text{at the surface,} \tag{14b}$$

where X_s is the value of X at the surface and X_b is taken as the value of X at the $z = 2$ m level above the surface for T and q and $V_b = V_s$, $V_s = 0$. The drag coefficient C_D is taken to be equal to 0.002 over ocean, 0.003 over low land below 1500 m and 0.005 over highland above 1500 m both for V and for T, while the vertical eddy diffusion coefficient K_z is considered to be given by the following lapse rate γ $(= -\frac{\partial T}{\partial z})$ dependent formula for V and T under convectively stable conditions:

$$K_z = \{5 + A[1 - \exp(10(\gamma_c - \gamma))]\} \cdot [1 + 0.3(k-1)] \text{ m}^2\text{s}^{-1}, \qquad \text{for } \gamma_c < \gamma \leqslant \gamma_d, \tag{15a}$$

$$K_z = \{3 + 2[1 + 10(\gamma_c - \gamma)]^{-1}\} \cdot [1 + 0.3(k-1)] \text{ m}^2\text{s}^{-1}, \qquad \text{for } \gamma \leqslant \gamma_c. \tag{15b}$$

where $\gamma_c = 6.0$ K/km, $\gamma_d = 10.0$ K/km, $k = 1,2,3,4$ is the model layer index and A is taken to be equal to 10 or 5 according to whether the diurnal variation of solar radiation is included or not. This formula is similar to those used by Deardorff[5], Washington and Kasahara[6] and Somerville et al.[7], and it is based on the assumption that the eddies transport sensible heat upward when the stratification γ is more unstable than the normal stratification γ_c and downward when γ is more stable than γ_c.

Since the mixing ratio q is calculated only once every 4 time steps, a smaller vertical diffusion coefficient is used for it and this K_z is taken to be given by the following simple expression both over land and over ocean under convectively stable conditions

$$K_z = 1 + 0.5(k-2) \text{ m}^2\text{s}^{-1}, \qquad \text{for } q. \tag{16}$$

In this work, we assume that the highland with elevation over 3000 m is wet, hence evaporation there is allowed. On the other hand, no evaporation is allowed over low land so that the effect of the soil moisture content of the ground on evaporation is not included. Thus, the general bulk evaporation rate from the surface is taken as

$$E = \eta \rho_s C_D |V_s| (q_s - q_b), \tag{17}$$

where C_D is taken to be equal to 0.002 everywhere in this equation but with the coefficient η given by

$$\eta = \begin{cases} 2 \text{ or } 1, & \text{for ocean,} \\ 0.1, & \text{for highlands over 3000 m in elevation,} \\ 0, & \text{for lands lower than 3000 m in elevation.} \end{cases} \tag{17a}$$

In our model, there are still other physical processes such as convective adjustment, solar and infrared rediations, large-scale condensation and deep cumulus convections and so on. However, we shall not describe the schemes of their inclusions here in order to save space. The readers who are interested in those schemes can refer to Kuo and Qian's papers [2,3].

3. *Horizontal Coordinate Systems and Topography*

Here in the global version of the model, we still use the spherical horizontal coordinates with $5° \times 5°$ grid size in both latitudes and longitudes between 65°S and 65°N. However, the grid size is changeable polewards, in order to keep quasi-constant distance between two adjacent points along latitudinal circles. At the poles, we use two Cartesian coordinate systems to treat the polar points as predictable and combine the spherical and the Cartesian coordinates together at 85° latitude. The details of the treatment can be found in [8]. Because of the combination of the two different horizontal coordinates at 85° and the different grid size in the spherical coordinates, reflection of some meteorological waves may take place and influence computational stability, therefore it is required to use some smoothing techniques. We utilize the so-called three-point zonal smoothing to suppress reflection waves.

This simulation is mainly contributed to the understanding of the influences of plateaus and mountains on diurnal changes of meteorological elements, therefore a nearly real topography must be used in the model shown in Fig.1 with the unit of decameters. From Fig.1, we see that the main orographic properties of the globe are considered. The physical properties of underlying surfaces are taken as the functions of orographic heights only. For example, the drag coefficient and albedo are changing only according to the surface heights above sea level and according to whether it is land or ocean. The albedo values are set to be equal to 10% for oceans, 20% for low land with elevation lower than 1500 m, 30% for land of elevation between 1500 m and 3000 m, and 40% for high land above 3000 m, if the temperature in the lowest layer of the atmosphere is below 0°C, then the albedo is taken to be equal to 70%. Nevertheless we get quite reasonable simulation and the simulated results are fairly in consistence with those of Kuo and Qian in the east hemisphere.

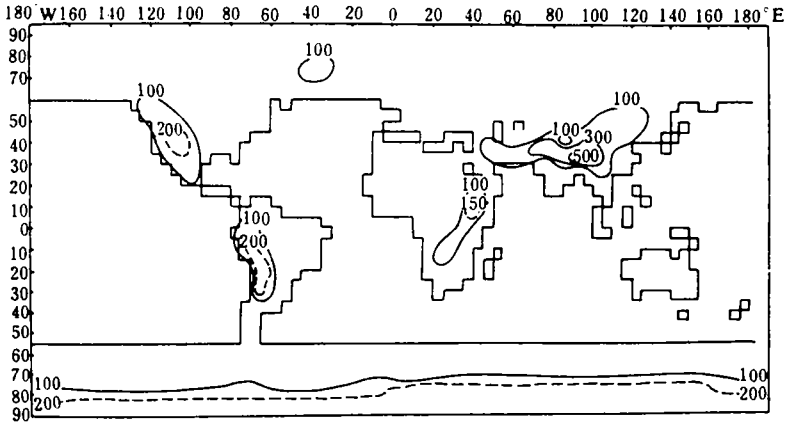

Fig. 1. Smoothed topography used in the global model in 10 m.

The initial data of the simulation are taken from the June zonal averaged pressure fields (see Kuo and Qian[2]). The starting time is taken as 18:00 local time at 90°E. The integration is conducted up to 6.5 days with day 6 assumed as daytime (nighttime) situation and day 6.5 as nighttime (daytime) situation in the Tibetan area (in the Rockies). The daily mean is obtained by the average from day 5.5 to day 6.5. In the next section, we shall discuss the daily mean results first in order to show the reliability of the experiment, and then emphatically discuss the influences of the Tibetan Plateau and the Rockies on diurnal variations of meteorological fields, such as geopotential height, temperature and winds.

III. DISCUSSIONS OF SIMULATED RESULTS

1. *The Daily Mean Fields*

Fig. 2 is the daily mean distribution of the sea-level pressure. It is easily seen that the simulated patterns in the Northern Hemisphere are more realistic than those in the Southern Hemisphere. The two monsoon depressions over the Tibetan Plateau and the Rockies and the two highs over the West Pacific and the Atlantic oceans are all fairly simulated. The two monsoon troughs over India and Indochina along the coastal areas are also realistically produced with their locations and strengths being in good consistence with the real ones. Even the extension of the Atlantic high to the Mediterranean can be seen in Fig.2. The low over the North America is simulated too deep, and so is the low over the north of the South America, but the main patterns of the two lows are still similar to the climatological ones. On the contrary, the two oceanic highs are simulated somewhat weaker and northward. The worst simulation is the high band along 30°S. It is perhaps caused by the coarseness of our considerations about the Antarctic Plateau.

At the 300 mb level, we produced a Tibetan high with its center located just above the Plateau, a North American high with a center at 110°W and 25°N.

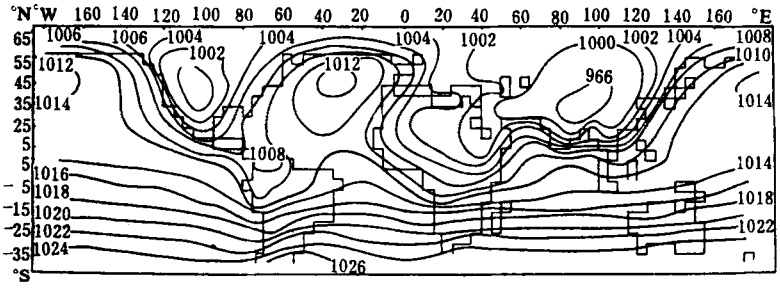

Fig. 2. Daily mean distribution of sea-level pressure in mb.

Fig. 3 is the daily mean precipitation amount distribution. It is shown that several maximum and minimum precipitation belts are all well simulated, especially the maximum belts to the southeast of the Tibet in the east of India Peninsula and in the west of Indochina. The maximum amount in the area to the south of the Tibet reaches 37 mm/day. In Arabian area a relative minimun amount region is produced, but with no break as the climatic one does. The precipitation amount on the lee side of the Rockies is undersimulated, this discrepancy might

result from the assumption that evaporation over land exists only when orographic heights exceed 3000 m, and the maximum height of the Rockies we used is just 2000 m. Therefore, there is no evaporation from the surface over the Rockies.

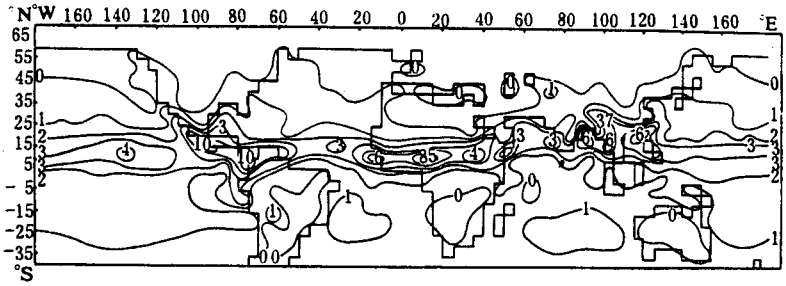

Fig. 3. Daily mean distribution of precipitation in mm/day.

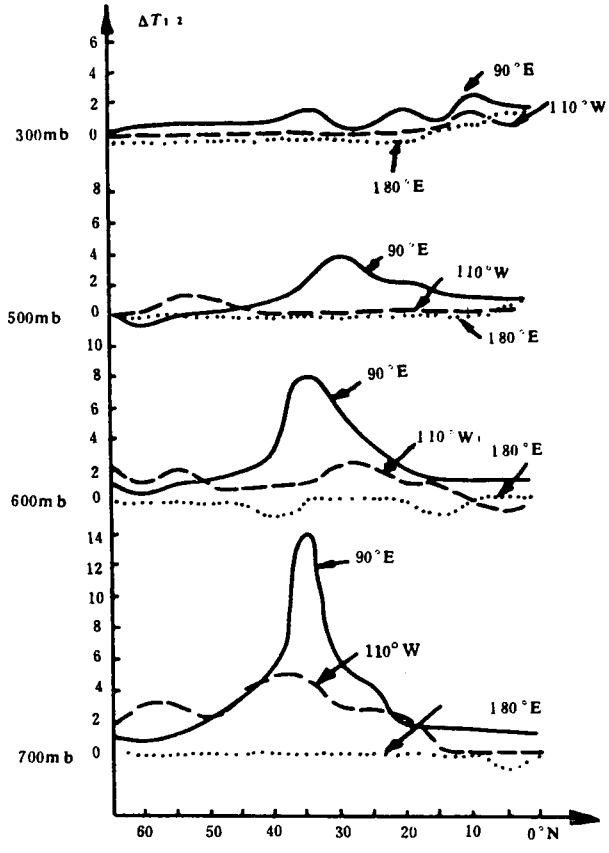

Fig. 4. Meridional profiles of the 12-hour changes of temperature along 90°E, 180°, and 110° W. Abscissa for latitudes and ordinate for temperature change ranges (K).

2. *Diurnal Variations of Temperature and Geopotential Height*

Fig. 4 is the meridional profiles of the 12-hour changes of temperature along 90°E, 180° and 110°W, with abscissa for latitudes and ordinate for temperature change ranges during 12 hours. The temperature changes represent the differences of the temperatures at 18:00 and 06:00 LST at 90°E, at 16:00 and 04:00 LST at 110°W and at 12:00 and 00:00 LST at 180°, respectively. From Fig.4 we see that there is no obvious diurnal variation in the whole troposphere over oceans (the amplitude less than 1 K), while there are very prominent diurnal variations in mountainous regions. The maximum amplitudes and the horizontal and vertical scales of the diurnal variations are all proportional to the scales of mountains. The maximum is 9° in the Plateau and 5° in the Rockies. The amplitudes decrease exponentially with height, the influence of the Tibetan Plateau can reach the 500 mb level with a 4° center over 90°E while that of the Rockies only reaches the 600 mb with amplitudes less than 2°. Besides, the area of obvious diurnal variations of temperature (defined as $\Delta T_{12} \geqslant 2°$) contracts with increasing height (not shown by figure). Those properties discussed above should be of importance in the weather and climate in mountainous areas.

The characteristics of the diurnal variations of geopotential height fields are the same as those of temperature. But the amplitudes of diurnal variations increase with height rather than decrease. In the Tibetan Plateau, there is a negative difference area at the 500 mb level, that means that the hot low in the area deepens at daytime. In the Rockies, there is no negative change even at the 700 mb because the scale and the height of the Rockies are much smaller and lower than those of the Tibetan Plateau.

3. *Horizontal Flows*

In order to get a complete understanding of the horizontal flows over the Tibetan Plateau and over the Rockies, we show the simulated flow patterns in the boundary layer of 50 mb thickness in Figs. 5(a) and 5(b).

Fig. 5(a) represents the daytime (nighttime) pattern and Fig. 5(b) the nighttime (daytime) pattern in the Tibetan Plateau (the Rockies).

From the comparison of Fig. 5(a) with 5(b), we know that the horizontal flow in mountains has prominent diurnal variation. At daytime, the air converges from outside to the mountain peak and diverges at nighttime. The convergent area over the Rockies is smaller than that over

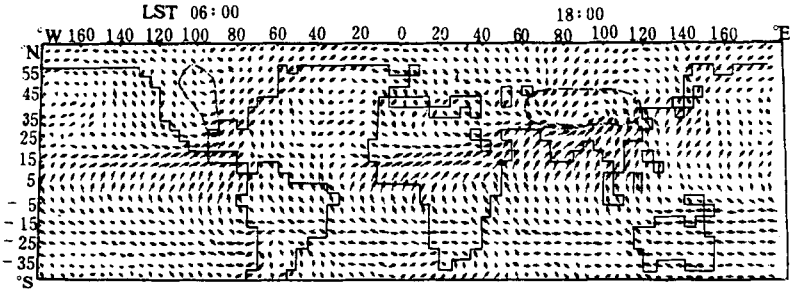

Fig. 5(a). Simulated flow patterns in the boundary layer at daytime (nighttime) in the Tibetan Plateau (in the Rockies). The area plotted by dotted lines represents mountain-valley wind area.

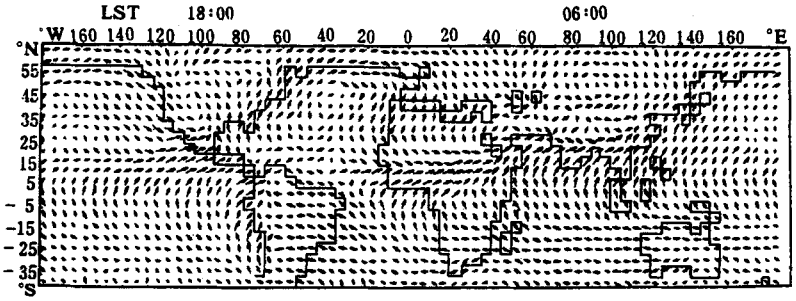

Fig. 5(b). As in Fig. 5(a) except for nighttime (daytime) in the Tibetan Plateau (in the Rockies).

the Plateau. The directions of convergent lines coincide with the directions of mountains, for instance, the convergent line over the Tibetan Plateau has a quasi-west-east direction and that over the Rockies has a NW-SE direction. On the contrary, the convergent line over the ocean (near 15°N, west hemisphere) has no evident diurnal change. Therefore, the prominent diurnal changing air flow is also a characteristic of mountains. The diurnal variation of horizontal flow will result in diurnal variation of vertical circulations, therefore, it has important effect on weather and climate too.

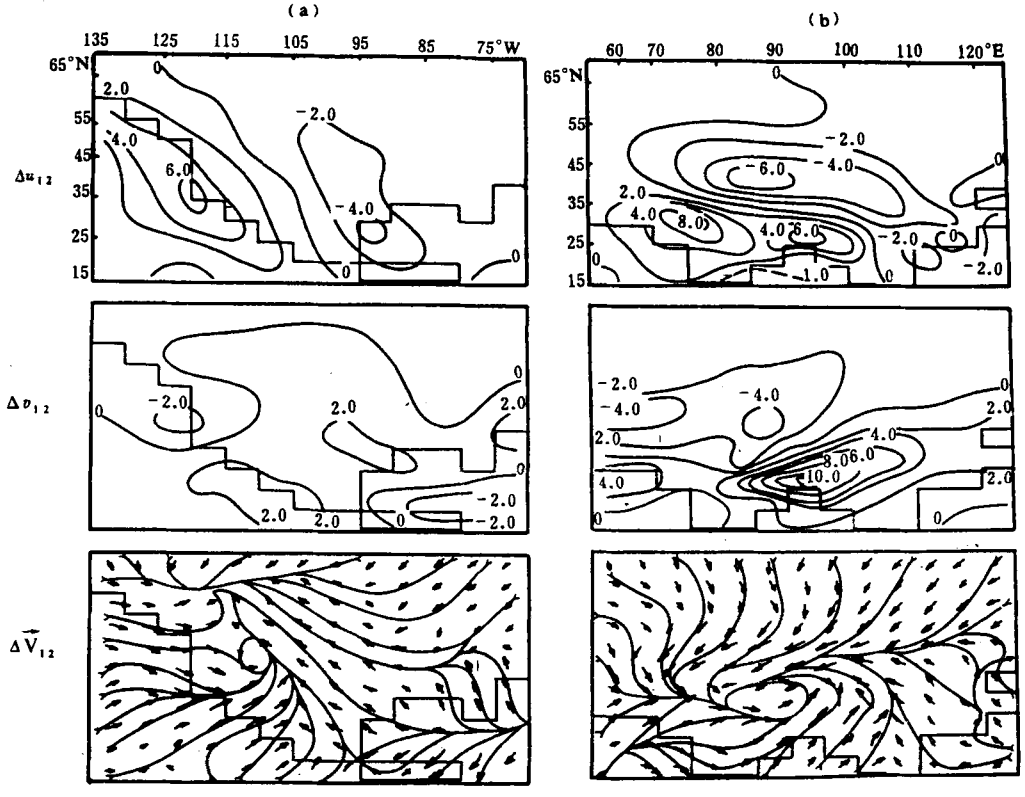

Fig. 6(a),(b). The 12-hour differences of u, v components and wind vector (m/s) at $\sigma_b = \frac{1}{2}$ in the Rockies (a) and in the Tibetan plateau (b)

We further define the mountain-valley winds according to the wind direction variation of more than 100°. By the definition, we find that the thickness of the mountain-valley wind over the Tibetan Plateau is about 1km and represented by the area with dotted lines in Fig. 5(a). At the $\sigma=0.75$ level, the area with mountain-valley winds contracts much to the interior of the Plateau (not shown by Figs.). We also find that the area to the south of the Plateau appears in a region where there is no evident mountain-valley wind, southwest flow prevails and the diurnal difference of the wind directions is less than 90°. The Rockies have the similar phenomena of mountain-valley winds and the area is also represented by dotted lines. It is clear that the scale of mountain-valley winds in the Rockies is smaller than that in the Tibetan Plateau, and is seen clearly only on the lee side of the mountains. The mountain-valley wind over the Iranian Plateau is altered by that over the Tibetan Plateau because the scale of the former is much smaller than that of the latter.

In order to get a quantitative analysis of the vertical distribution of the diurnal wind variation, we calculated the 12-hour differences of the u and v components at the coordinate surfaces, and then we composed them to get the 12-hour wind vector differences at the same surfaces. We find that in the lower layers the diurnal variation of v component over the Tibetan Plateau is more prominent than that of u component, and the case is just reverse over the Rockies (see Figs. 6(a) and 6(b)). That is to say, the different orientations of mountains have different effects on wind variations. However, there are some similarities, one of which is that the

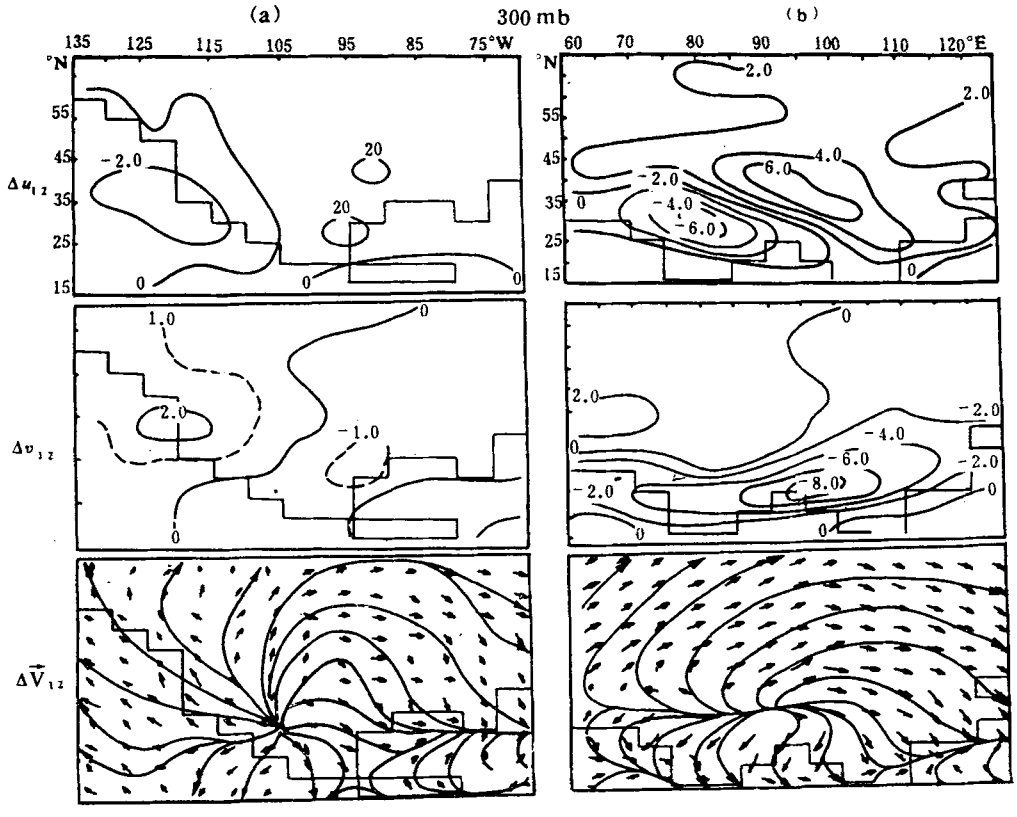

Fig. 7(a), (b). As in Fig. 6(a), (b) except for the 300mb level.

differential wind vector is always towards the crests of mountains, therefore a cyclonic circulation of differential winds is found there, of course, because of the differential heating at daytime and at nighttime. Figs. 7(a) and 7(b) represent the diurnal variations at 300mb level. we find that the diurnal variations of winds both over the Tibetan Plateau and over the Rockies are tremendously reduced. We can see another characteristic from Figs. 7(a) and 7(b), that is, the differential wind vectors in the lower layers are towards the mountains while those in the upper layers towards outside. It is also resulted from the diurnal variations of the heating fields.

4. *Vertical Motion*

Figs. 8(a) and 8(b) represent the 12-hour variations of the vertical velocities over the Tibetan Plateau and over the Rockies. It is clear that the diurnal amplitudes of the vertical velocities are much larger over the Plateau than those over the Rockies. From Figs. 8(a) and 8(b) and other Figs. (not shown here), it is clear that , at daytime, the upward motion prevails over the Plateau and the complementary downward motion in the vicinities; the case is reversed aloft at nighttime. Over the adjacent oceans of the Tibetan Plateau downward motion is prominent. Over the Rockies, the upward motion prevails everywhere except over a small area to the east of 90°W, the complementary downward motion exists over the adjacent oceans or over the coastal area of the land. The maximum amplitudes over the two mountainous areas are both at the $\sigma=0.25$ level in the σ-coordinate part.

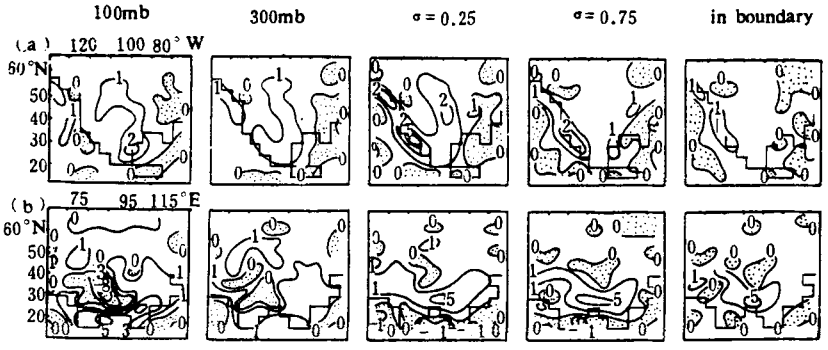

Fig. 8(a),(b). The 12-hour variations of the vertical velocities (cm/s) over the Rocky Mountains (a) and over the Tibetan Plateau (b). Dotted area represents downward motion.

5. *Vertical Circulations*

Figs.9(a) and 9(b) are the meridional vertical circulations along 110°W, 90°E and 180°, respectively, at daytime (a) and at nighttime (b). It is seen that there are evident monsoon circulations in the Rockies, in the Tibetan Plateau and in the Pacific ocean. At daytime the monsoon circulation over the south of the Rockies has a maximum upward branch near 20°—25°N, and a maximum downward branch near 10°S. The maximum upward branch of the monsoon circulation over the Tibetan Plateau appears near 30°—35°N, even at 45°N there is still an apparent upward motion, the downward branch is located at 15°S. The maximum value of the upward motion over the Tibetan area is about 4 times larger than that over the Rockies. In sharp contrast, the monsoon circulation over the Pacific ocean has a maximum upward branch near 10°N and a downward branch near 10°S, these two branches are both weak with the upward motion being even 5 times weaker than that over the Rockies. At the same time, we

find that the monsoon circulations over the mountainous areas have more evident diurnal variations than that over the ocean, especially at the south sides of the mountains. At nighttime, there appears a small and narrow vertical circulation just at the south slopes, while to the south of 20°N, there still exists a monsoon circulation like that at daytime but with weaker vertical motions.

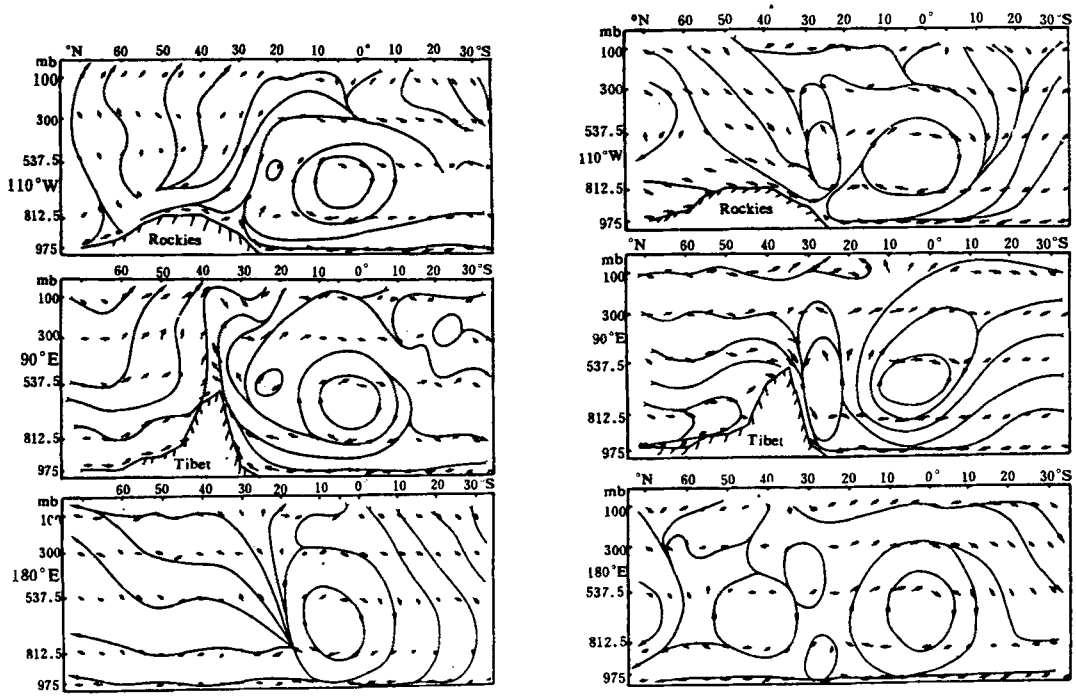

Fig. 9(a), (b). The meridional vertical circulations along 110°W (top), 90°E (middle), and 180° (bottom) at daytime (a) and at nighttime (b), respectively. The vertical velocity is magnified 100 times.

IV. CONCLUSIONS

From the above discussions, we get some preliminary conclusions as follows:

(1) The evident diurnal variations of the temperature, the geopotentials, the horizontal and the vertical motions, and the vertical circulations are the special characteristics in mountainous regions. The horizontal and the vertical scales of the influences of mountains and the diurnal amplitudes are all proportional to the scale and the height of topography. Therefore, the Tibetan Plateau has greater influence than the Rockies.

(2) The diurnal amplitudes of temperature over the Tibetan Plateau and over the Rocky mountains exponentially decrease with increasing height, while those of geopotentials increase. The maximum variation of temperature is 9°C over the Tibetan area and 5°C over the Rockies. The diurnal amplitudes of temperature over oceans keep lower than 2°C.

(3) The diurnal changes of winds are also proportional to the orographic scale and height, mountains result in an increasing convergent field in lower layers and an increasing corresponding divergent field aloft. The convergent line has a similar direction with the mountain.

(4) Evident mountain-valley winds exist over the Tibetan Plateau and the Rockies with a thickness of about 1km. The mountain-valley wind over the Tibet is the strongest, next comes that over the Rockies, while the mountain-valley wind on the east slope of the Iranian Plateau is altered by that over the Tibetan Plateau.

(5) Vertical motions over mountains have prominent diurnal variations. The upward motion appears at daytime and the downward motion at nighttime. The upward motion over the Rockies has downward complementary motion only over oceans and along coasts, while the upward motion over the Tibetan Plateau has complementary downward motion not only over oceans but also in the vicinities nearby.

(6) The vertical monsoon circulations to the south sides of the Tibetan Plateau and the Rocky mountains are critically influenced by the mountains. The orographic substances intensify the circulations at daytime and weaken them at nighttime with an induced small vertical circulation located on the south slopes.

REFERENCES

[1] 叶笃正,高由禧,青藏高原气象学,科学出版社,1979.

[2] Kuo, H. L. & Qian Yongfu, *Mon. Wea. Rev.*, **109** (1981), 11, 2337—2356.

[3] kuo, H. L. & Qian Yongfu, *Mon. Wea. Rev.*, **110** (1982), 12, 1879—1897.

[4] 钱永甫,颜宏,骆启仁,王谦谦,大气科学,1978,2,91—102.

[5] Deardorff, J. W., *J.Appl. Meteor.*, **6** (1967), 631—643.

[6] Washington & Kasahara, *Mon. Wea. Rev.*, 98(1970). 559-580.

[7] Somerville et al., *J. Atmos. Sci.*, **31** (1974), 84—117.

[8] 钱永甫,王谦谦,高原气象,1983,1,1—15.